CHEMISTRY OF MATERIALS
Cite This: Chem. Mater. 2020, 32, 195−204
Article
pubs.acs.org/cm

Designing High Performance Nonfullerene Electron Acceptors with Rylene Imides for Efficient Organic Photovoltaics

Nagesh B. Kolhe,[†,‡] Sarah M. West,[†,‡] Duyen K. Tran,[†,‡] Xiaomei Ding,[†] Daiki Kuzuhara,[§] Noriyuki Yoshimoto,[§] Tomoyuki Koganezawa,[∥] and Samson A. Jenekhe*[,†]

[†]Department of Chemical Engineering and Department of Chemistry, University of Washington, Seattle, Washington 98195-1750, United States

[§]Faculty of Science and Engineering, Iwate University, 4-3-5 Ueda, Morioka, Iwate 020-8551, Japan

[∥]Industrial Application Division, Japan Synchrotron Radiation Research Institute, Sayo, Hyogo 679-5198, Japan

Supporting Information

ABSTRACT: Improving carrier mobility, redox stability, blend morphology, and photovoltaic performance while elucidating structure−property relationships remains an important design goal for nonfullerene electron acceptors (NFAs) for organic solar cells. Although numerous NFAs have been created from rylene diimide electron-deficient building blocks, they have shown far inferior photovoltaic properties compared to benchmark fused-ring electron acceptors (FREAs) such as ITIC. Herein we show that new bis(naphthalene-imide)arylenelidenes (BNIAs), incorporating rylene-imide end-capping groups via methine bridges in donor−acceptor architectures, are endowed with enhanced electrochemical redox stability, high carrier mobilities, and high photovoltaic performance. Pairing of those BNIAs that are also FREAs, NIDT and NIBT, respectively, with donor polymer PBDB-T produced 10.0−10.8% efficient photovoltaic devices, which are comparable to benchmark ITIC devices. Blends of FREAs NIDT and NIBT and those of non-FREA NITV were found to have similar electron mobilities, demonstrating that the much higher photovoltaic efficiency of NIDT and NIBT devices does not originate from enhanced charge transport but from differences in blend morphology and blend photophysics. The results demonstrate that incorporating rylene imides into molecular architectures through the methine-bridged donor−acceptor coupling motif is a promising design strategy toward more efficient and electrochemically rugged materials for organic solar cells.

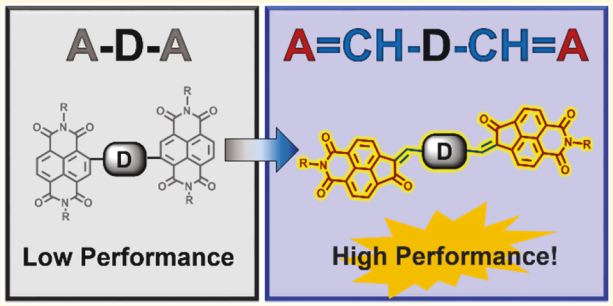

INTRODUCTION

Considerable progress has been made in organic photovoltaics (OPVs) in the last 5 years as a result of advances in the design and synthesis of nonfullerene electron acceptors (NFAs).[1−15] Single-junction solar cells produced from small-molecule NFAs have achieved power conversion efficiencies (PCEs) of 14−16%.[7−11] The PCEs of even all-polymer solar cells utilizing polymeric NFAs have also exceeded 10%.[12−15] The linear acceptor−donor−acceptor molecular architecture has proved to be an essential feature of highly efficient small-molecule NFAs.[1−4] Polycyclic fused ring structures such as indaceno[2,1-*b*:6,5-*b*′]dithiophene (IDT) and indacenodithieno[3,2-*b*]thiophene (IDTT) have become the standard donor moieties in the design of a class of NFAs often termed fused ring electron acceptors (FREAs).[1−4] Although various end-capping acceptor units such as indandione,[16,17] rhodanine,[16,18−24] malononitrile,[25,26] barbiturate,[27] and their derivatives[2] have been widely explored, recent efforts have mainly focused on 1,1-dicyanomethylene-3-indanone (DCMI)[28,29] and its halogenated derivatives[2,30] which have produced the current best performing NFAs.[9−11] However, these high performing NFAs or FREAs generally lack reversible redox processes,[9,28,29] which is essential to the intrinsic stability of the materials, and their electron mobility remains a major limitation on achievable PCEs of OPV devices.[31] There is thus a need to explore alternative electron-deficient units toward increasing electrochemical redox stability, enhancing electron mobility and better understanding of structure−property relationships of NFAs.

Rylene diimides and rylene imides are among the most widely investigated electron-deficient building blocks for constructing both polymeric[32−34] and small-molecule semiconductors[1,2] for OPVs and organic electronic applications due to their many benefits, including high electron affinity, high electron mobility,[33] tunable optical and electronic properties,[35,36] and high thermal and electrochemical redox stability.[2,32,33] Although numerous NFAs with donor−acceptor structures containing rylene diimide (RyDI), notably perylene

Received: August 16, 2019
Revised: November 27, 2019
Published: December 2, 2019

DOI: 10.1021/acs.chemmater.9b03329
Chem. Mater. 2020, 32, 195−204

diimide (PDI),[37−40] naphthalene diimide (NDI),[39,41,42] tetraazabenzodifluoranthene diimide (BFI),[5,6,43,44] and naphtho[2,3-*b*]thiophene diimide (NTI),[45] have been reported, only a few have resulted in OPV devices with a PCE exceeding 8%.[6,45] Even in linear acceptor−donor−acceptor structures, such as NDI−IDTT−NDI or PDI−IDT−PDI,[46,47] where the donor moieties are identical to those in the high performing DCMI-containing NFAs and FREAs, the PCEs of the former were only 2−7%.[46−48] We hypothesize that the generally inferior performance of all current RyDI-containing NFAs, compared to those containing DCMI and derivatives, is due to the difference in the donor−acceptor coupling motif, which influences molecular planarity, electronic structure, carrier mobility, photophysics, intermolecular interactions, etc. In the cases of acceptor−donor−acceptor NFA triads containing RyDI moieties, the coupling motif is best represented as A−D−A in which there is no bridging group between the donor and the acceptor moieties;[1,2,4,45,47,48] such NFAs have generally been made by Stille or Suzuki type reactions.[45,47,48] In contrast, similar high-performance NFA triads containing DCMI or derivatives and exemplified by indacenodithieno[3,2-*b*]-thiophene end-capped with two DCMI units (ITIC) have generally been made by Knoevenagel condensation,[1,2,9,49] and should strictly be best described to have an A═CH−D−CH═A coupling motif, wherein a methine group bridges the acceptor and donor moieties. Heretofore, examples of the latter donor−acceptor coupling motif containing an RyDI or RyI have not been reported. Here, we further explore this hypothesis experimentally.

In this paper, we report the synthesis and investigation of the first examples of NFAs with an **A═CH−D−CH═A** donor−acceptor coupling motif containing rylene-imide electron-deficient end-capping units. We show that the new NFAs, bis(naphthalene-imide)arylenelidenes (BNIAs), whose molecular structures are given in Chart 1, include those that can be regarded as FREAs (NIDT and NIBT) and one that has a nonfused ring donor moiety (NITV), but all have highly planar molecular conformations, exhibit highly reversible electrochemical redox processes, and have similar electronic structures. An important novel feature of the BNIAs compared to other NFAs with A═CH−D−CH═A architecture is the alkyl chains on the naphthalene imide end groups that provide opportunity for tuning solubility, blend morphology, and photovoltaic properties. Blends of the new BNIAs containing fused ring donor moieties, NIDT and NIBT, respectively, with the donor polymer PBDB-T, exhibit high photovoltaic efficiencies (>10%) that are comparable to those of DCMI-containing NFAs.[50,51] Neat films and photovoltaic blends of FREAs NIDT and NIBT were found to have carrier mobilities comparable to those of the non-FREA NITV, implying that the enhanced photovoltaic efficiency of FREAs does not originate from the enhanced charge transport. The superior photovoltaic performance of the FREAs NIDT and NIBT compared to non-FREA NITV is accounted for by the observed differences in blend morphology and blend photophysics in favor of the FREAs. These results on BNIAs are in good agreement with the above donor−acceptor coupling motif hypothesis and suggest that rylene imides are promising electron-deficient building blocks for the design of NFAs with improved properties and enhanced redox stability.

Chart 1. Molecular Structures of BNIAs

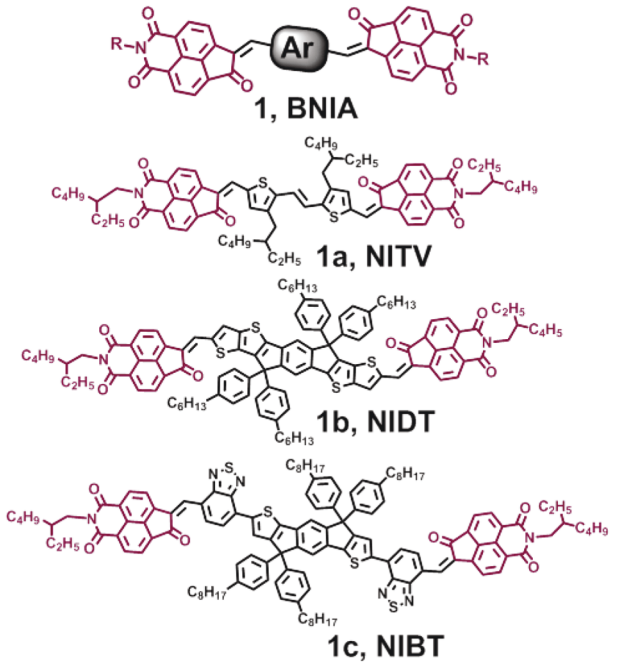

RESULTS AND DISCUSSION

Synthesis, Optical, and Electrochemical Properties. The new BNIAs, including NITV, NIDT, and NIBT (Chart 1), were synthesized by Knoevenagel condensation of a dialdehyde functionalized donor moiety and a naphthalene imide (NI) bearing a keto-methylene group as shown in Scheme S1, and the detailed procedures and characterization data are given in the Materials and Methods section below and in the Supporting Information (SI). The end-capping monoketone-NI was synthesized by the previously reported procedure.[43,52] The electron donor intermediates (IDTT-CHO and IDTBT-CHO) were synthesized in good yields following literature procedures.[21,28,53] TVT was synthesized following a literature procedure[54] and formylated as described in the Materials and Methods section. All the BNIAs are readily soluble in common solvents (chloroform, dichloromethane, chlorobenzene, etc.), and their molecular structures were confirmed by ^{1}H NMR, ^{13}C NMR, and MALDI-TOF mass (Figures S1−S11). Theoretically, three different isomers (cis−cis, cis−trans, and tans−trans) could be expected for each of the BNIAs (Figures S12−S14). Two different isomers were isolated using standard column chromatography, resulting in major (63−72%) and minor (37−28%) isomers for each of the BNIAs; a third, possible isomer was not present in a measurable quantity. All subsequent characterizations and studies focused on the major isomer of each BNIA. The BNIAs exhibit good thermal stability (5% weight loss at >350 °C) in nitrogen atmosphere, as measured by thermogravimetric analysis (Figure S15). None of the BNIAs exhibit melting or crystallization peaks in differential scanning calorimetry (DSC) scans up to 300 °C (Figure S16).

The optical absorption spectra of the BNIAs in chloroform solutions (Figure 1a) had peaks in the 567−628 nm region with maximum extinction coefficients of 8.4×10^4 to 1.1×10^5 M^{-1} cm^{-1} (Table 1). The absorption spectra are slightly broadened in thin films with a red-shifted peak in NIDT and NIBT but a blue-shifted peak in NITV (Figure 1b). The red-shifted absorption spectra of NIDT and NIBT indicate

DOI: 10.1021/acs.chemmater.9b03329
Chem. Mater. 2020, 32, 195−204

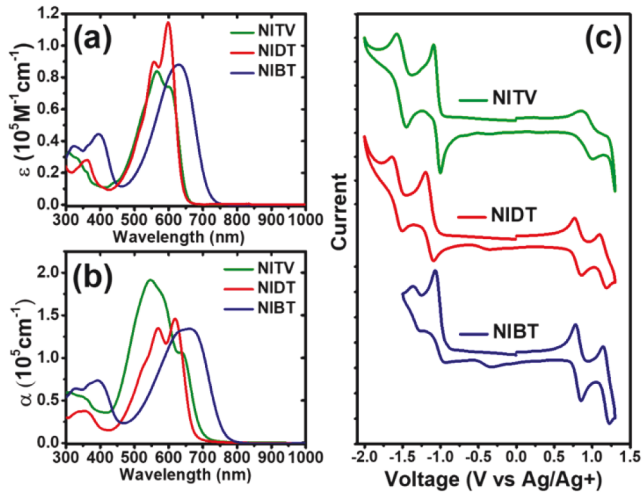

Figure 1. Absorption spectra of BNIAs in chloroform solution (a) and as thin films on glass substrates (b). Cyclic voltammograms of BNIAs in 0.1 M $BuNPF_6$ dichloromethane solutions at 100 mV/s scan rates (c).

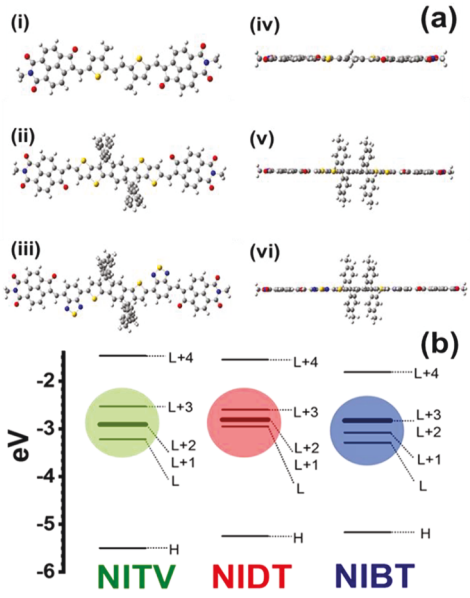

Figure 2. (a) Top view (i, ii, iii) and side view (iv, v, vi) of the optimized geometries from DFT calculations at the B3LYP/6-31G(d) level (2-ethylhexyl groups were replaced with methyl groups): (i and iv) NITV, (ii and v) NIDT, and (iii and vi) NIBT. (b) Calculated quasi-degenerate LUMO energy levels of the optimized BNIAs from DFT calculations (B3LYP/6-31G(d)).

enhanced intramolecular charge transfer due to the improved self-organization induced by the central ring donor moieties. In contrast, the blue-shifted thin film absorption of NITV suggests H-aggregation[55] or a less planar conformation in the thin film.[56] The thin-film absorption edge optical bandgap varies from 1.63 eV in NIBT to 1.85 eV in NIDT (Table 1). The solution and thin-film photoluminescence (PL) emission spectra of the BNIAs had peaks centered at 650−732 nm and 637−771 nm, respectively (Figure S17).

We characterized the electrochemical redox processes of the BNIAs by cyclic voltammetry in dichloromethane solution (Figure 1c). The observed cyclic voltammograms (CVs) show that all three BNIAs exhibit two reversible reduction waves with excellent stability in many cycles as expected from the NI building blocks.[42,57] Similar to donor−acceptor molecules in our previous work,[58] the reversible redox waves in BNIAs can be assigned to the formation of stable radical anions on the naphthalene-imide and radical cations on the donor moiety, respectively, with possible subsequent delocalization over the entire molecule. This means that both electrons and holes could be injected and transported in each of the BNIAs. Finally, the HOMO/LUMO energy levels extracted from the onset redox potentials, using $E_{HOMO/LUMO} = -(4.8 + E_{ox/red}^{1/2})$ eV, are collected in Table 1.

Theoretical Calculations. We performed density functional theory (DFT) calculations at the B3LYP/6-31G(d) level of theory to gain better understanding of the molecular geometry and distribution of the frontier molecular orbitals in the new BNIAs (Figure 2a and Figures S18−S20). The optimized geometries show that the BNIAs have highly planar backbones while the molecular orbital distributions show that the HOMO energy levels are distributed primarily along the core donor moiety and the LUMO energy levels are more delocalized across the whole molecule. To further understand the electron accepting abilities of the new BNIA molecules, the frontier molecular orbital energy levels were calculated at the same B3LYP/6-31G(d) level (Figures S18−S20). We found that each of the molecules (NITV, NIDT, and NIBT) has four quasi-degenerate LUMO levels that are closely spaced. NITV, NIDT, and NIBT have four LUMOs that are banded together by 0.69, 0.35, and 0.46 eV, respectively (Figure 2b). These initial simulation results suggest that the newly developed BNIAs have a higher density of states at the LUMO than $PC_{60}BM$[59] and thus that they have potential superior electron accepting properties.

Nonfullerene Organic Solar Cells. We selected the widely used donor polymer PBDB-T (Figure 3a) to investigate the photovoltaic properties of the new BNIAs. The normalized absorption spectra of PBDB-T and the three NFAs show that there is complete overlap with both NITV and NIDT while NIBT has a red-shifted absorption relative to PBDB-T (Figure 3b). In terms of achieving complementary contributions to light harvesting from both donor polymer and NFA, PBDB-T is clearly not ideal, especially for NITV and NIDT with which the polymer has complete overlap in absorption spectra (Figure 3b). However, the electronic energy level offsets at each BNIA:PBDB-T interface (Figure 3c) are adequate for

Table 1. Optical Properties, Electronic Structure, Thermal Stability, and SCLC Carrier Mobilities of the BNIAs

BNIA	λ_{max} [a] (nm)	ε_{max} (M^{-1} cm^{-1})	λ_{max} [b] (nm)	E_g (eV)	HOMO (eV)	LUMO (eV)	T_d [c] (°C)	μ_e (cm^2/(V s))	μ_h (cm^2/(V s))
NITV	567	8.4×10^4	548	1.78	−5.40	−3.62	369	8.83×10^{-5}	9.90×10^{-5}
NIDT	599	1.1×10^5	618	1.85	−5.34	−3.58	368	4.65×10^{-5}	6.41×10^{-5}
NIBT	628	8.8×10^4	660	1.63	−5.38	−3.68	354	1.44×10^{-4}	1.41×10^{-4}

[a]Absorption maximum in chloroform solution (10^{-6} M). [b]Spin-coated thin films from chloroform solution. [c]5% weight loss from TGA.

DOI: 10.1021/acs.chemmater.9b03329
Chem. Mater. 2020, 32, 195−204

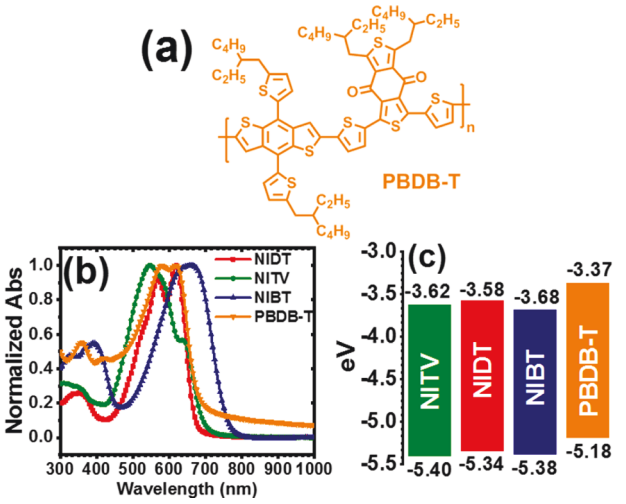

Figure 3. (a) Molecule structure of PBDB-T donor polymer. (b) Normalized thin film optical absorption spectra of PBDB-T and BNIAs. (c) HOMO/LUMO energy levels of donor polymer and BNIA acceptors.

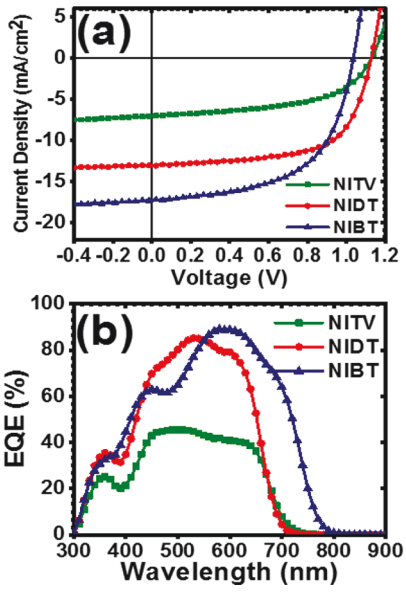

Figure 4. (a) Current density (J_{sc})−voltage (V) curves for the optimized BNIA:PBDB-T solar cells. (b) EQE spectra for the optimized BNIA:PBDB-T solar cells.

both efficient photoinduced electron transfer and photoinduced hole transfer.[2,60]

The photovoltaic properties of the new BNIAs were characterized by fabricating solar cells with an inverted architecture: ITO/ZnO/PEI/Blend/MoO_3/Ag, where polyethyleneimide (PEI) is the cathode interface layer.[61] NITV:PBDB-T blend active layers were prepared under optimized conditions of a 2.5:1 (w/w) blend ratio, spin coating from chlorobenzene solutions *without* the use of any solvent processing additive, and thermal annealing at 160 °C for 10 min. The optimal device processing conditions for NIDT:PBDB-T blend devices consisted of a 1.2:1 (w/w) blend ratio, spin-coating from chlorobenzene solution *with* 0.5% (v/v) diiodooctane (DIO) as the solvent additive, and thermal annealing at 120 °C for 10 min. NIBT:PBDB-T blend devices consisted of a 1.2:1 (w/w) blend ratio, spin-coating from chlorobenzene solution *with* 1.0% (v/v) DIO as the solvent additive, and thermal annealing at 140 °C for 10 min. The current density−voltage (J−V) curves and the external quantum efficiency (EQE) spectra of these devices are shown in Figure 4a,b, respectively, whereas the corresponding photovoltaic parameters (J_{sc}, V_{oc}, FF, and PCE) are collected in Table 2.

Devices fabricated from NITV:PBDB-T blends had a maximum PCE of 4.8% with a high V_{oc} of 1.13 V accompanied by a modest J_{sc} of 7.02 mA/cm^2 and FF of 0.54 (Table 2). In contrast, NIDT:PBDB-T and NIBT:PBDB-T blend devices were found to have over 2-fold enhancement in the overall performance. Notably, the J_{sc} values increased to 13.01 mA/cm^2 in NIDT devices and to 17.20 mA/cm^2 in NIBT-based devices (Table 2). The much-enhanced photocurrent in NIBT devices can be understood to arise from its red-shifted absorption spectrum compared to the other NFAs and the PBDB-T donor polymer. The fill factor of the NIDT and NIBT devices had enhanced values of 0.66 and 0.60, respectively. The improvement in the FF can be ascribed to the optimal blend morphology with smaller domain sizes as found by 2D GIWAXS and AFM characterization to be discussed later. It is to be noted that all the devices based on the new NFAs have V_{oc} above 1 V, which is rarely observed in high performing organic solar cells.[7−9,11] The high V_{oc} values of 1.04−1.13 V are due to the high-lying LUMO energy levels of the BNIAs. The combination of moderately high J_{sc} and FF without compromising the V_{oc} enabled NIDT- and NIBT-based devices to achieve maximum PCEs of 10.0% and 10.8%, respectively.

The external quantum efficiency (EQE) spectra of the optimized BNIA-based devices (Figure 4b) showed onset of photocurrent generation at 800 nm for the NIBT devices and at 700 nm for the NITV and NIDT devices in excellent agreement with the absorption spectra. The maximum EQE values, 45.4% for NITV devices, 85.3% for NIDT devices, and 89.1% for NIBT devices, were found in the 510−580 nm region. The integrated photocurrents calculated from the EQE spectra are in good agreement with the J−V measurements (Table 2), showing less than a 5% mismatch. Notably, the EQE spectra show that photocurrent generation is much lower in the 300−500 nm range due to the poor absorption of both the new NFAs and the PBDB-T donor polymer. This suggests that improved performance could be expected from the new NFAs if paired with a donor polymer with a complementary absorption.

The charge recombination dynamics of the BNIA:PBDB-T blend devices was examined by measuring the short-circuit current (J_{sc}) and the open-circuit voltage (V_{oc}) as a function of the incident light intensity (P_{light}). As shown in Figure 5a, the expected power-law dependence of J_{sc} on P_{light} ($J_{sc} \propto P_{light}^{\alpha}$) was observed with the α values that slightly deviated from unity (α = 0.94−1.02), which is indicative of suppressed bimolecular recombination.[62] On the other hand, a linear relationship between V_{oc} and P_{light} is expected with the slope of $1kT/q$ and $2kT/q$ representing bimolecular recombination and trap-assisted recombination, respectively.[62] The data (Figure 5b) show that the charge recombination kinetics in NIDT- and NIBT-based devices were primarily governed by trap-assisted recombination ($s \sim 2kT/q$), whereas NITV-based devices had mixed bimolecular and trap-assisted recombinations (s = 1.3 kT/q).

DOI: 10.1021/acs.chemmater.9b03329
Chem. Mater. 2020, 32, 195−204

Table 2. Photovoltaic Properties and SCLC Carrier Mobilities of the Optimized BNIA:PBDB-T Blend Devices[a]

blend	J_{sc} ($J_{sc}^{calc.}$) (mA/cm^2)	V_{oc} (V)	FF	PCE (%)	μ_e (cm^2/(V s))	μ_h (cm^2/(V s))
NITV:PBDB-T	8.08 (7.6) (7.02 ± 0.71)	1.12 (1.13 ± 0.01)	0.53 (0.54 ± 0.03)	4.8 (4.3 ± 0.30)	1.91×10^{-5}	1.13×10^{-4}
NIDT:PBDB-T	13.28 (12.8) (13.01 ± 0.28)	1.14 (1.13 ± 0.02)	0.66 (0.64 ± 0.01)	10.0 (9.5 ± 0.30)	2.11×10^{-5}	1.54×10^{-4}
NIBT:PBDB-T	17.34 (16.5) (17.20 ± 0.25)	1.04 (1.04 ± 0.01)	0.60 (0.58 ± 0.01)	10.8 (10.4 ± 0.21)	1.58×10^{-5}	6.91×10^{-4}

[a]Average values with a standard deviation were obtained from 16 devices.

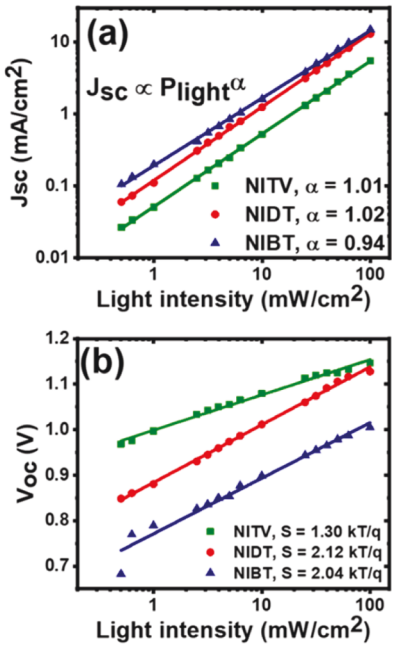

Figure 5. (a) J_{sc} dependence on light intensity for BNIA:PBDB-T blends. (d) V_{oc} dependence on light intensity for BNIA:PBDB-T blends. All active layers were processed at optimized device conditions.

Exciton dissociation and charge collection dynamics were also investigated by analyzing the relationship between the photocurrent ($J_{ph} = J_{light} - J_{dark}$) and the effective voltage ($V_{eff} = V_{bias} - V_{applied}$) (Figure S18). The nonsaturated J_{ph} in the NITV-based devices at a high voltage of 2 V (Figure S21a) suggested a high degree of geminate recombination.[62,63] This observation might be explained by the large domain sizes observed in AFM images of NITV:PBDB-T blends, thus, hindering efficient exciton diffusion and exciton dissociation.[64] In contrast, NIDT- and NIBT-based devices exhibited saturated J_{ph} even at a low voltage of about 0.8 V, suggesting efficient photoinduced charge carrier generation rate (G_{max}) of about 10^{25}–10^{26} m^3/s (Figure S21b,c). Moreover, the charge collection probabilities calculated at the short-circuit condition, $P(E, T)$, in NIDT- and NIBT-based devices were 94.8% and 92.8%, respectively, which are superior to that of NITV-based devices ($P(E, T)$ = 84.8%). This finding is consistent with the observed lower J_{sc} and FF in NITV-based devices as compared to NIDT- and NIBT-based devices.

Bulk Charge Transport Properties of Neat BNIA Films and Blend Active Layers. We measured the electron and hole mobilities of the BNIA neat films and the BNIA:PBDB-T blend films by the space-charge limited current (SCLC) method using two configurations: ITO/ZnO/PEI/Active layer/Al for electron-only devices and ITO/PEDOT:PSS/Active layer/MoO_3/Ag for hole-only devices. The SCLC fittings for the neat films and the blend films are shown in Figures S22 and S23, respectively. The SCLC carrier mobilities for neat films and blend films are included in Tables 1 and 2, respectively. We observed balanced ambipolar charge transport in neat films of the new BNIAs with electron mobility (μ_e) and hole mobility (μ_h) that average around 5×10^{-5}–10^{-4} cm^2/(V s). In particular, the μ_e varied from 1.44×10^{-4} cm^2/(V s) in NIBT films to 4.65×10^{-5} cm^2/(V s) in NIDT films (Table 1). The same trend was also observed for the hole mobility, which varies from 1.41×10^{-4} cm^2/(V s) for NIBT films to 6.41×10^{-5} cm^2/(V s) for NIDT films (Table 1). The balanced ($\mu_h/\mu_e \sim 1$) ambipolar charge transport observed in neat films of the BNIAs is understood from the upshifted HOMO energy level (HOMO ~ −5.4 eV), which could facilitate hole injection. The ability to efficiently transport both holes and electrons simultaneously, especially in the neat NIBT films, suggested the potential for also developing OPV devices without a bulk heterojunction architecture.

In the case of BNIA:PBDB-T blend films, the bulk electron mobility decreased relative to those of the neat films. The electron mobilities in all three blends were comparable to each other (μ_e = (1.6–2.1) × 10^{-5} cm^2/(V s)), with the highest electron mobility observed in NIDT blends (Table 2). The hole mobility in the blend films varied from 6.91×10^{-4} cm^2/(V s) in NIBT devices to 1.54×10^{-4} cm^2/(V s) in NIDT blends and to 1.13×10^{-4} cm^2/(V s) in NITV blends. Clearly, charge transport characteristics in all BNIA blends are unbalanced ($\mu_h/\mu_e \gg 1$), which could explain the moderate FF values (0.53–0.66) observed in the photovoltaic properties.[62,63] The asymmetric charge transport in the BNIA blend devices suggests that further optimization of the morphology and choice of a different donor polymer could allow the full potential of this new class of NFA materials to be realized.

The observed bulk charge transport properties of both the neat BNIA thin films and the photovoltaic blends have remarkable features. First, the finding that the electron mobility of NITV:PBDB-T blends is similar to the μ_e values in the NIDT:PBDB-T and NIBT-PBDB-T blends means that charge transport is not among the factors limiting the photovoltaic efficiency of NITV devices compared to the NIDT and NIBT devices. Second, the finding that neat films and blends of FREAs NIDT and NIBT have carrier mobilities comparable to those of the corresponding neat films and blends of non-FREA NITV means that the benefits of the semiladder structure of FREAs do not originate from the enhanced charge transport. Although ladder and semiladder structures in organic semiconductors can significantly enhance carrier mobilities in general,[65,66] the present BNIAs all have highly planar molecular conformations as found in DFT calculations discussed above and the 2D GIWAXS results to be discussed below show that the π–π intermolecular stacking distance is similar in NITV, NIDT, and NIBT.

Surface and Bulk Morphology of Active Layer Blends. Atomic force microscopy (AFM) imaging of the surface morphology of neat and blend films of the BNIAs (Figures S24 and S25) showed that NITV neat films had distinctive granular

DOI: 10.1021/acs.chemmater.9b03329
Chem. Mater. 2020, 32, 195–204

morphology with large crystallites and rough surface (R_q = 5.4 nm) whereas neat NIDT and NIBT films had smoother surfaces (R_q ~ 1−3 nm) and a homogeneous fibrillar morphology. NITV:PBDB-T blend films revealed suboptimal morphology with large domain sizes of about 140 nm (Figure S25). NIDT and NIBT blend films showed smaller domain sizes of about 30−40 nm (Figure S25), which suggest a more beneficial morphology for efficient exciton diffusion, exciton dissociation, and charge transport properties, in agreement with the observed photovoltaic properties.

Thin-film crystallinity, molecular ordering, and morphology of the neat BNIAs and their binary blends with PBDB-T were characterized by 2D grazing-incidence wide-angle X-ray scattering (GIWAXS) measurements (Figure 6 and Figures S26−27). Neat BNIA thin-films showed significant crystallinity as seen from the intense diffraction peak line cuts in both the in-plane (IP) and out-of-plane (OOP) directions (Figure S26). The 2D GIWAXS pattern of NITV shows a ring-like feature, and its 1D line-cut profile shows a ring-like feature and lamellar (100) and π-stacking (010) peaks in both IP and OOP directions, corresponding to d-spacings of 18.47 and 3.65 Å (Table S1), respectively. These results indicate that the NITV neat film had mixed edge-on and face-on molecular packing. NIDT crystallites show preferential face-on molecular orientation as seen from the strong (100) peak at q_{xy} = 0.41 Å (d-spacing = 15.31 Å) in the IP direction and a sharp (010) peak at q_z = 1.79 Å (d-spacing = 3.50 Å) in the OOP direction. Similarly, NIBT shows face-on packing with a (100) peak at q_{xy} = 0.25 Å (d-spacing = 25.12 Å) and (010) peak at q_z = 1.74 (d-spacing = 3.60 Å). The calculated crystal coherence length (CCL) from the (100) lamellar peak was 4.6−6.8 nm for all the BNIAs. A similarly calculated CCL of 5.8 nm was obtained from the GIWAXS patterns of neat PBDB-T (Figure S27) in accordance with literature reports.[67]

The 2D GIWAXS patterns and 1D line-cut profiles for BNIA:PBDB-T blend films (Figure 6a,b) show that the (010) π-stacking peak in the OOP direction and (100) lamellar peak in the IP direction can be assigned to face-on molecular packing. In particular, the lamellar (100) peak in the IP direction from both NIDT and PBDB-T can be clearly observed in the NIDT:PBDB-T blend film, along with intense (010) stacking peak in the OOP direction, which implies that both NIDT and PBDB-T have maintained their face-on orientation in the blend. Moreover, the reduced CCL of 4.82 nm compared to the neat film suggests compatibility between NIDT and PBDB-T. Although PBDB-T maintained its preferential face-on packing in all the blends in good agreement with the observed high hole mobilities (6.91−1.13 × 10^{-4} $cm^2/(V\ s)$), the molecular orientations of NITV and NIBT changed upon blending with PBDB-T. In the NITV:PBDB-T blend, the intensity of the (100) peak in the OOP direction is decreased relative to the neat NITV film, which suggests that some fraction of the NITV molecules has changed into face-on packing in the blend. However, in the NIBT:PBDB-T blends, a sharp (100) peak in the OOP direction emerged, which suggests that some NIBT molecules adopt edge-on packing in the blend. Overall, the 2D GIWAXS results show that the type of donor moiety incorporated into the A═CH−D−CH═A motif greatly impacts the crystallinity and molecular packing of BNIA molecules.

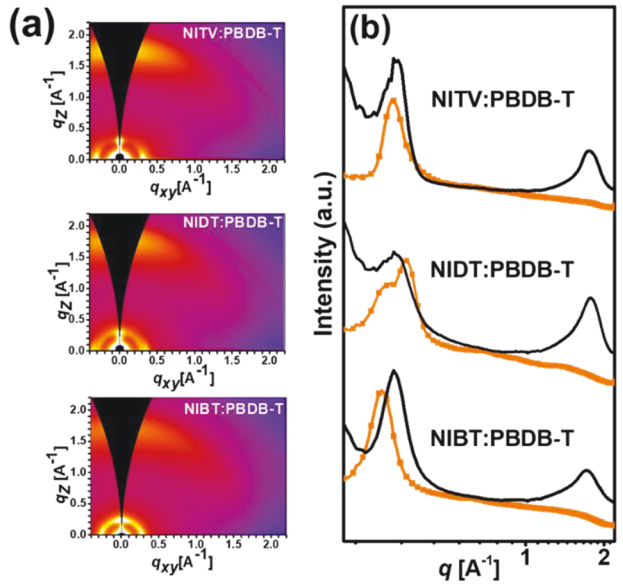

Figure 6. (a) 2D GIWAXS patterns of BNIA:PBDB-T optimal blend films. (b) Corresponding in-plane (orange line with symbol) and out-of-plane (black solid line) line-cut profiles.

CONCLUSIONS

In summary, we have designed and synthesized bis-(naphthalene imide)arylenelidenes (BNIAs) to test the hypothesis that incorporating rylene imides as the electron-deficient end-capping units in methine-bridged donor−acceptor architectures could lead to high performance in OPV devices. We found that OPV devices from NIDT:PBDB-T and NIBT:PBDB-T blends combine high V_{oc} (>1 V) and high PCEs of up to 10.0 and 10.8%, respectively. The new BNIAs, NIDT and NIBT, were found to combine the characteristic reversible redox processes of rylene imides with the planarity, strong intramolecular charge transfer, and high photovoltaic performance commonly seen in other NFAs with a methine-bridged donor−acceptor coupling motif. We have found that neat films and photovoltaic blends of FREAs NIDT and NIBT respectively have comparable carrier mobilities as those of the non-FREA NITV, demonstrating that the observed enhanced photovoltaic efficiency of FREAs does not originate from enhanced charge transport. The substantially enhanced photovoltaic properties of FREAs NIDT and NIBT, with fused ring donor moieties, compared to non-FREA NITV is due to the large domains in the phase-separated blend morphology, mixed *face-on* and *edge-on* molecular orientations, mixed bimolecular and trap-assisted recombinations, and reduced charge collection probability in the NITV:PBDB-T blends. Our results demonstrate that incorporating rylene imides into molecular architectures with a methine-bridged donor−acceptor coupling motif is a promising design strategy toward more efficient and electrochemically rugged OPV materials.

MATERIALS AND METHODS

Materials. Thieno[3,2-*b*]thiophene, diethyl 2,5-dibromotereph-thalate, anhydrous THF, 2.5 M *n*-butyllithium in hexanes, anhydrous $ZnCl_2$, $Pd(PPh_3)_4$, 4-hexyl-1-bromobenzene, glacial acetic acid, sulfuric acid, sodium hydroxide, anhydrous DMF, acenaphthalene, polyetheleneimine (PEI), dimethylcarbamoyl chloride, aluminum trichloride, anhydrous chlorobenzene, hydrochloric acid, absolute ethanol, 2-ethylhexylamine, phosphorus oxychloride, acetic anhydride,

DOI: 10.1021/acs.chemmater.9b03329
Chem. Mater. 2020, 32, 195−204

chromium(VI) oxide, anhydrous chloroform, 1,2-dichloroethane, and anhydrous piperidine were purchased from Sigma-Aldrich and used without further purification. The donor polymer PBDB-T was synthesized in our lab according to the published literature procedure.[68] The compound NI-monoketone (Scheme S1) was synthesized by slight modification of the literature method[43,52] as detailed below. The donor moiety intermediate TVT[54] was synthesized according to the literature prodecure and formylated as detailed below. The other donor moieties IDTT-CHO[28] and IDTBT-CHO[21] (Scheme S1) were synthesized following literature methods.

Synthesis of [2-(2-Ethylhexyl)-1H-indeno[6,7,1-def]isoquinoline-1,3,6(2H,7H)-trione] (NI-monoketone). 2-(2-Ethylhexyl)-6,7-dihydro-1*H*-indeno[6,7,1-*def*]isoquinoline-1,3(2*H*)-dione[52] (4.0 g, 12.0 mmol) and acetic anhydride (250 mL) were combined and gently heated until fully dissolved. After cooling to room temperature, chromium(VI) oxide (1.79 g, 18.0 mmol) was added in three portions over 1 h. The green mixture was stirred at room temperature for 3−4 h. Then, the mixture was poured into ice. After the ice melted, the mixture was extracted with chloroform. The combined extracts were washed with sodium bicarbonate thoroughly and dried over Na_2SO_4 before purifying with silica gel column chromatography using hexane:dichloromethane (5:2, v/v) to elute a pale yellow solid (1.08 g, 26% yield). ^{1}H NMR (300 MHz, $CDCl_3$, δ): 8.68 (d, J = 8.0 Hz, 1H), 8.59 (d, J = 8.0 Hz, 1H), 8.14 (d, J = 8.0 Hz, 1H), 7.75 (d, J = 8.0 Hz, 1H), 4.17 (m, 2H), 4.00 (s, 2H), 1.96 (m, 1H), 1.39 (m, 8H), 0.95 ppm (m, 6H). ^{13}C NMR (500 MHz, $CDCl_3$, δ): 199.73, 163.71, 163.42, 141.41, 140.87, 137.80, 132.56, 131.59, 125.63, 125.52, 122.15, 121.91, 120.244, 44.03, 42.32, 37.71, 30.45, 28.65, 23.76, 22.77, 13.80, 10.36. ESI-MS (m/z): calcd. for $C_{22}H_{23}NO_3$, 349.17; found, 349.30.

Synthesis of (E)-5,5′-(Ethene-1,2-diyl)bis(4-(2-ethylhexyl)-thiophene-2-carbaldehyde (TVT-CHO). Under nitrogen, (*E*)-1,2-bis(3-(2-ethylhexyl)thiophen-2-yl)ethene[54] (1.02 g, 2.45 mmol) and DMF (0.4 g, 5.39 mmol) were combined in a reaction flask, dissolved in 1,2-dichloroethane (10 mL), and cooled down to 0 °C. To the solution was added $POCl_3$ (0.83 g, 5.39 mmol) dropwise. The reaction mixture was kept at 0 °C for 15 min and was warmed up to room temperature. The reaction mixture was then refluxed overnight. After cooling to room temperature, the mixture was poured into ice water and hydrolyzed with 20 mL of 2 M NaOH (aq). The mixture was warmed to 45 °C, stirred for 1 h, and extracted with chloroform. The organic layer was washed with water and brine and dried over anhydrous Na_2SO_4 before purifying with silica gel column chromatography using dichloromethane to elute a yellow solid (0.98 g, 84.7% yield). ^{1}H NMR (300 MHz, $CDCl_3$, δ): 9.84 (s, 2H), 7.50 (s, 2H), 7.23 (s, 2H), 2.62 (d, J = 7.02 Hz, 4H), 1.64−1.47 (m, 2H), 1.30 (m, 16H), 0.91 (m, 12H). ^{13}C NMR (500 MHz, $CDCl_3$, δ): 182.65, 145.66, 142.86, 140.48, 139.36, 122.38, 41.19, 32.67, 32.49, 28.86, 25.69, 23.03, 14.10, 10.95. ESI-MS (m/z): calcd. for $C_{28}H_{40}O_2S_2$, 472.25; found, 473.10.

Synthesis of NIDT. Under nitrogen, NI-monoketone (0.350 g, 0.93 mmol) and IDTT-CHO (0.250 g, 0.23 mmol) were combined in a reaction flask. Then, anhydrous chloroform (50 mL) was added and the mixture was stirred until dissolved. Piperidine (0.238 g, 0.28 mL) was then added, and the mixture was stirred at 50−55 °C for 24 h. The reaction mixture was cooled to room temperature, poured into water containing 3−4% HCl (v/v), extracted with dichloromethane, washed with water, and dried over Na_2SO_4. After removal of the solvent, the crude material was purified by silica gel column chromatography with hexane:dichloromethane (1:4, v/v) to yield a purple solid (0.350 g, 87% yield). ^{1}H NMR (300 MHz, $CDCl_3$, δ): 8.67 (d, J = 7.42 Hz, 2H), 8.58 (d, J = 7.42 Hz, 2H), 8.28 (s, 2H), 8.16 (d, J = 7.30 Hz, 2H), 7.85 (d, J = 7.55 Hz, 2H), 7.76 (s, 2H), 7.62 (s, 2H), 7.25−7.15 (m, 16H), 4.15 (m, 4H), 2.58 (t, 8H), 1.95 (m, 2H), 1.61 (m, 8H), 1.30 (m, 46H), 0.87 ppm (m, 24H). ^{13}C NMR (500 MHz, $CDCl_3$, δ): 189.87, 163.76, 163.51, 154.54, 148.89, 146.81, 142.01, 142.33, 142.27, 141.99, 139.27, 139.23, 137.12, 136.34, 135.26, 132.78, 131.73, 131.24, 130.99, 128.49, 127.76, 126.71, 125.31, 125.52, 121.94, 119.83, 117.62, 116.08, 63.88, 43.99, 37.82, 35.36, 31.43, 31.92, 30.75, 29.69, 28.92, 28.45, 24.06, 23.08, 22.30, 13.80, 10.41. MALDI-TOF (m/z): [M$^+$] calcd. for $C_{114}H_{116}N_2O_6S_4$,1737.77; found, 1737.31. Anal. Calcd. for $C_{114}H_{116}N_2O_6S_4$: C, 78.76; H,6.73; N, 1.61. Found: C, 76.04; H, 6.46; N, 1.62%.

Synthesis of NITV. Synthesis was carried out using similar procedures as mentioned above using NI-monoketone (0.590 g, 1.68 mmol), TVT-CHO (0.200 g, 0.43 mmol), and piperidine (0.428 g, 0.496 mL). The crude material was purified by silica gel column chromatography with hexane:dichloromethane (1:5, v/v) to yield a greenish solid (0.306 g, 65% yield). ^{1}H NMR (300 MHz, $CDCl_3$, δ): 8.60 (d, J = 7.30 Hz, 2H), 8.47 (d, J = 7.42 Hz, 2H), 8.09 (d, J = 7.30 Hz, 2H), 7.75 (d, J = 7.42 Hz, 2H), 7.62 (s, 4H), 7.33 (s, 2H), 4.10 (m, 4H), 2.73 (d, 4H), 1.93 (m, 24H), 1.68 (m, 24H), 1.41−1.27 (m, 32H), 0.95 ppm (m, 24 H). ^{13}C NMR (500 MHz, $CDCl_3$, δ): 189.44, 163.45, 163.30, 146.75, 142.9, 142.90, 142.65, 142.01, 141.99, 138.01, 137.80, 136.98, 135,77, 135.46, 135.15, 132.50, 131.41, 129.02, 126.72, 125.15, 125.08, 122.20, 121.89, 121.75, 121.49, 119.73, 115.85, 43.93, 41.58, 41.32, 40.97, 37.80, 32.52, 30.48, 28.83, 28.44, 25.87, 24.02, 22.83, 13.84, 10.87, 10.37. MALDI-TOF (m/z): [M$^+$] calcd. for $C_{72}H_{82}N_2O_6S_2$,1134.54; found, 1134.25. Anal. Calcd. for $C_{72}H_{82}N_2O_6S_4$: C, 76.16; H,7.28; N, 2.47. Found: C, 75.82; H, 7.05; N, 2.55%.

Synthesis of NIBT. Synthesis was carried out using similar procedures as mentioned above using NI-monoketone (0.465 g, 0.133 mmol), IDTBT-CHO (0.410 g, 0.333 mmol), and piperidine (0.225 g, 0.263 mL). The crude material was purified by silica gel column chromatography with hexane:dichloromethane (1:9 v/v) to yield a dark purple color solid (0.312 g, 50% yield). ^{1}H NMR (300 MHz, $CDCl_3$, δ): 9.49 (d, 1H), 8.76−8.61 (m, 4H), 8.46 (m,1H), 8.28−8.15 (m, 6H), 8.03 (m, 4H), 7.61 (s,2H), 7.31−7.41 (m, 16H), 4.17 (m, 4H), 2.60 (m, 8H), 1.97 (m, 2H), 1.61 (m, 8H), 1.32−1.27 (m, 56H), 0.87 ppm (m, 24 H). ^{13}C NMR (500 MHz, $CDCl_3$, δ): 190.19, 163.70, 163.50, 157.26, 155.23, 154.55, 154.30, 154.12, 151.68, 151.43, 142.30, 141.41, 141.36, 141.13, 138.04, 137.14, 136.20, 135.60, 133.58, 132.82, 132.57, 131.61, 128.38, 128.17, 127.58, 125.39, 123.67, 122.40, 121.93, 121.04, 120.49, 118.16, 117.91, 62.97, 44.04, 37.82, 37.75, 35.38, 31.62, 31.44, 30.73, 29.41, 28.98, 28.40, 24.05, 22.81, 22.39, 13.84, 10.41, 10.35. MALDI-TOF (m/z): [M$^+$] calcd. for $C_{130}H_{136}N_6O_6S_4$,2005.94; found, 2005.49. Anal.: Calc. for $C_{130}H_{136}N_6O_6S_4$: C, 77.81; H,6.83; N, 4.19. Found: C, 77.20; H, 6.66; N, 4.46%.

Fabrication and Characterization of BNIA-Based Polymer Solar Cells. OPV devices were fabricated with an inverted architecture of ITO/ZnO/PEI/Blend/MoO_3/Ag. ITO-coated substrates (15 Ω/square, Shanghai B. Tree Tech, Shanghai, China) were cleaned sequentially in ultrasonic baths with acetone, deionized water, and isopropyl alcohol for 30 min, dried using nitrogen gas, and followed by 90 s of O_2 plasma cleaning. The ZnO precursor solution was spin-coated onto the ITO substrates at 5300 rpm for 40 s, followed by thermal annealing at 250 °C for 30 min to make an ∼30 nm thick ZnO layer. A 0.05 wt % solution of polyethylenimine (PEI) in 2-methoxyethanol was spin-coated onto the ZnO layer and dried at 120 °C for 10 min. Subsequently, NITV:PBDB-T (2.5:1, w/w), NIDT:PBDB-T (1.2:1, w/w), and NIBT:PBDB-T (1.2:1 w/w) blends were prepared in chlorobenzene, mixed, and stirred overnight at 80 °C in the glovebox. The 0% DIO (v/v), 0.5% (v/v), and 1% (v/v) of DIO solvent additive was used for the NITV, NIDT, and NIBT blends, respectively. The blend solution of NITV, NIDT, and NIBT was spin-coated at 1000 rpm for 50 s, followed by thermal annealing at 160 °C for 10 min, 120 °C for 10 min, and 140 °C for 10 min, respectively, in the glovebox. All the active layers had a thickness of 99 ± 5 nm. MoO_3 (7.5 nm) and Ag (100 nm) were thermally deposited onto the blend active layer. Each substrate contained four devices, each with an active area of 9 mm^2. An aperture mask with area of 3.14 mm^2 was applied during measurements to define the illuminated device area. The photovoltaic cells were tested under AM 1.5G solar illumination at 100 mW/cm^2 in ambient air by using a solar simulator (Model 16S, Solar Light Co., Philadelphia, PA) with a 200 W xenon lamp power supply (Model XPS 200, Solar Light Co., Philadelphia, PA) calibrated by an NREL certified Si photodiode (model 1787-04,

DOI: 10.1021/acs.chemmater.9b03329
Chem. Mater. 2020, 32, 195−204

Hamamatsu Photonics K.K., Japan) and a HP4155A semiconductor parameter analyzer (Yokogawa Hewlett-Packard, Japan).

Fabrication and Characterization of SCLC Devices. Current−voltage ($J-V$) characteristics of the SCLC devices were measured by using a HP4155A semiconductor parameter analyzer (Yokogawa Hewlett-Packard, Tokyo). The carrier mobility was deduced by fitting the $J-V$ curves to the Mott−Gurney equation where J is the current density, ε_0 is the permittivity of free space, ε is the relative permittivity, μ is the zero-field mobility, V is the applied voltage, and d is the thickness of active layer:

$$J = \frac{9}{8}\varepsilon\varepsilon_0\mu\frac{V^2}{d^3}$$

The SCLC device structures for electron-only and hole-only devices were ITO/ZnO/PEI/Blend/Al (100 nm) and ITO/PEDOT:PSS/Blend/MoO_3 (7.5 nm)/Ag (100 nm), respectively. Each neat and blend active layer was processed at the optimized conditions for the OPV devices as described above and spin-coated at 1000 rpm for 50 s, which was followed by thermal annealing inside the glovebox.

■ ASSOCIATED CONTENT

Supporting Information

The Supporting Information is available free of charge at https://pubs.acs.org/doi/10.1021/acs.chemmater.9b03329.

Characterization of NI-monoketone, NITV, NIDT, and NIBT, NMR spectra, MALDI-TOF spectra, TGA traces, DSC scans, PL spectra, DFT electronic distributions, $J_{ph}-V_{eff}$ curves, SCLC fittings, AFM images, and 2D-GIWAXS patterns (PDF)

Special Issue Paper

This paper was submitted as a part of the Jean-Luc Bredas Festschrift, published as *Chemistry of Materials* Vol. 31, issue 17.

■ AUTHOR INFORMATION

Corresponding Author

*(S.A.J.) E-mail: jenekhe@u.washington.edu.

ORCID

Nagesh B. Kolhe: 0000-0003-2794-6122
Duyen K. Tran: 0000-0002-3065-6153
Daiki Kuzuhara: 0000-0001-7948-8501
Samson A. Jenekhe: 0000-0002-0898-9541

Author Contributions

‡(N.B.K., S.M.W., and D.K.T.) These authors contributed equally.

Notes

The authors declare no competing financial interest.

■ ACKNOWLEDGMENTS

We thank the Office of Naval Research (N00014-17-1-2203) and the National Science Foundation (CBET- 1803245) for support. N.B.K and D.K.T were supported by ONR and S.M.W and X.D were supported by NSF. The synchrotron radiation-based 2D-GIWAXS experiments were performed at the BL46XU and BL19B2 of SPring-8 with the approval of the Japan Synchrotron Radiation Research Institute (JASRI) (Proposal Nos. 2018A1744 and 2018B1772). The DFT calculations were done through the use of advanced computational, storage, and networking infrastructure provided by the Hyak supercomputer system at the University of Washington.

■ REFERENCES

(1) Yan, C.; Barlow, S.; Wang, Z.; Yan, H.; Jen, A. K. Y.; Marder, S. R.; Zhan, X. Non-fullerene acceptors for organic solar cells. *Nat. Rev. Mater.* **2018**, *3*, 18003.

(2) Zhang, G.; Zhao, J.; Chow, P. C. Y.; Jiang, K.; Zhang, J.; Zhu, Z.; Zhang, J.; Huang, F.; Yan, H. Nonfullerene Acceptor Molecules for Bulk Heterojunction Organic Solar Cells. *Chem. Rev.* **2018**, *118*, 3447−3507.

(3) Nielsen, C. B.; Holliday, S.; Chen, H.-Y.; Cryer, S. J.; McCulloch, I. Non-Fullerene Electron Acceptors for Use in Organic Solar Cells. *Acc. Chem. Res.* **2015**, *48*, 2803−2812.

(4) Hou, J.; Inganas, O.; Friend, R. H.; Gao, F. Organic Solar Cells Based on Non-Fullerene Acceptors. *Nat. Mater.* **2018**, *17*, 119−128.

(5) Li, H.; Earmme, T.; Ren, G.; Saeki, A.; Yoshikawa, S.; Murari, N. M.; Subramaniyan, S.; Crane, M. J.; Seki, S.; Jenekhe, S. A. Beyond Fullerenes: Design of Nonfullerene Acceptors for Efficient Organic Photovoltaics. *J. Am. Chem. Soc.* **2014**, *136*, 14589−14597.

(6) Hwang, Y.-J.; Li, H.; Courtright, B. A. E.; Subramaniyan, S.; Jenekhe, S. A. Nonfullerene Polymer Solar Cells with 8.5% Efficiency Enabled by a New Highly Twisted Electron Acceptor Dimer. *Adv. Mater.* **2016**, *28*, 124−131.

(7) Zhang, S.; Qin, Y.; Zhu, J.; Hou, J. Over 14% Efficiency in Polymer Solar Cells Enabled by a Chlorinated Polymer Donor. *Adv. Mater.* **2018**, *30*, 1800868.

(8) Zhang, H.; Yao, H.; Hou, J.; Zhu, J.; Zhang, J.; Li, W.; Yu, R.; Gao, B.; Zhang, S.; Hou, J. Over 14% Efficiency in Organic Solar Cells Enabled by Chlorinated Nonfullerene Small-Molecule Acceptors. *Adv. Mater.* **2018**, *30*, 1800613.

(9) Yuan, J.; Zhang, Y.; Zhou, L.; Zhang, G.; Yip, H.-L.; Lau, T.-K.; Lu, X.; Zhu, C.; Peng, H.; Johnson, P. A.; Leclerc, M.; Cao, Y.; Ulanski, J.; Li, Y.; Zou, Y. Single-Junction Organic Solar Cell with over 15% Efficiency Using Fused-Ring Acceptor with Electron-Deficient Core. *Joule* **2019**, *3*, 1140−1151.

(10) Fan, B.; Zhang, D.; Li, M.; Zhong, W.; Zeng, Z.; Ying, L.; Huang, F.; Cao, Y. Achieving over 16% efficiency for single-junction organic solar cells. *Sci. China: Chem.* **2019**, *62*, 746−752.

(11) Cui, Y.; Yao, H.; Zhang, J.; Zhang, T.; Wang, Y.; Hong, L.; Xian, K.; Xu, B.; Zhang, S.; Peng, J.; Wei, Z.; Gao, F.; Hou, J. Over 16% efficiency organic photovoltaic cells enabled by a chlorinated acceptor with increased open-circuit voltages. *Nat. Commun.* **2019**, *10*, 2515.

(12) Yao, H.; Bai, F.; Hu, H.; Arunagiri, L.; Zhang, J.; Chen, Y.; Yu, H.; Chen, S.; Liu, T.; Lai, J. Y. L.; Zou, Y.; Ade, H.; Yan, H. Efficient All-Polymer Solar Cells based on a New Polymer Acceptor Achieving 10.3% Power Conversion Efficiency. *ACS Energy Lett.* **2019**, *4*, 417−422.

(13) Kolhe, N. B.; Tran, D. K.; Lee, H.; Kuzuhara, D.; Yoshimoto, N.; Koganezawa, T.; Jenekhe, S. A. New Random Copolymer Acceptors Enable Additive-Free Processing of 10.1% Efficient All-Polymer Solar Cells with Near-Unity Internal Quantum Efficiency. *ACS Energy Lett.* **2019**, *4*, 1162−1170.

(14) Li, Z.; Ying, L.; Zhu, P.; Zhong, W.; Li, N.; Liu, F.; Huang, F.; Cao, Y. A generic green solvent concept boosting the power conversion efficiency of all-polymer solar cells to 11%. *Energy Environ. Sci.* **2019**, *12*, 157−163.

(15) Meng, Y.; Wu, J.; Guo, X.; Su, W.; Zhu, L.; Fang, J.; Zhang, Z.-G.; Liu, F.; Zhang, M.; Russell, T. P.; Li, Y. 11.2% Efficiency all-polymer solar cells with high open-circuit voltage. *Sci. China: Chem.* **2019**, *62*, 845−850.

(16) Srivani, D.; Gupta, A.; Bhosale, S. V.; Puyad, A. L.; Xiang, W.; Li, J.; Evans, R. A.; Bhosale, S. V. Non-fullerene acceptors based on central naphthalene diimide flanked by rhodanine or 1,3-indanedione. *Chem. Commun.* **2017**, *53*, 7080−7083.

(17) Winzenberg, K. N.; Kemppinen, P.; Scholes, F. H.; Collis, G. E.; Shu, Y.; Birendra Singh, T.; Bilic, A.; Forsyth, C. M.; Watkins, S. E. Indan-1,3-dione electron-acceptor small molecules for solution-processable solar cells: a structure-property correlation. *Chem. Commun.* **2013**, *49*, 6307−6309.

DOI: 10.1021/acs.chemmater.9b03329
Chem. Mater. 2020, 32, 195−204

(18) Baran, D.; Ashraf, R. S.; Hanifi, D. A.; Abdelsamie, M.; Gasparini, N.; Röhr, J. A.; Holliday, S.; Wadsworth, A.; Lockett, S.; Neophytou, M.; Emmott, C. J. M.; Nelson, J.; Brabec, C. J.; Amassian, A.; Salleo, A.; Kirchartz, T.; Durrant, J. R.; McCulloch, I. Reducing the efficiency-stability-cost gap of organic photovoltaics with highly efficient and stable small molecule acceptor ternary solar cells. *Nat. Mater.* **2017**, *16*, 363−369.
(19) Kim, Y.; Song, C. E.; Moon, S.-J.; Lim, E. Rhodanine dye-based small molecule acceptors for organic photovoltaic cells. *Chem. Commun.* **2014**, *50*, 8235−8238.
(20) Wu, Y.; Bai, H.; Wang, Z.; Cheng, P.; Zhu, S.; Wang, Y.; Ma, W.; Zhan, X. A planar electron acceptor for efficient polymer solar cells. *Energy Environ. Sci.* **2015**, *8*, 3215−3221.
(21) Holliday, S.; Ashraf, R. S.; Wadsworth, A.; Baran, D.; Yousaf, S. A.; Nielsen, C. B.; Tan, C.-H.; Dimitrov, S. D.; Shang, Z.; Gasparini, N.; Alamoudi, M.; Laquai, F.; Brabec, C. J.; Salleo, A.; Durrant, J. R.; McCulloch, I. High-efficiency and air-stable P3HT-based polymer solar cells with a new non-fullerene acceptor. *Nat. Commun.* **2016**, *7*, 11585.
(22) Holliday, S.; Ashraf, R. S.; Nielsen, C. B.; Kirkus, M.; Röhr, J. A.; Tan, C.-H.; Collado-Fregoso, E.; Knall, A.-C.; Durrant, J. R.; Nelson, J.; McCulloch, I. A Rhodanine Flanked Nonfullerene Acceptor for Solution-Processed Organic Photovoltaics. *J. Am. Chem. Soc.* **2015**, *137*, 898−904.
(23) Zou, Y.; Wu, Y.; Yang, H.; Dong, Y.; Cui, C.; Li, Y. The effect of alkylthio side chains in oligothiophene-based donor materials for organic solar cells. *Mol. Syst. Des. Eng.* **2018**, *3*, 131−141.
(24) Lee, T.; Eom, Y.; Song, C. E.; Jung, I. H.; Kim, D.; Lee, S. K.; Shin, W. S.; Lim, E. Simple Bithiophene-Rhodanine-Based Small Molecule Acceptor for Use in Additive-Free Nonfullerene OPVs with Low Energy Loss of 0.51 eV. *Adv. Energy Mater.* **2019**, *9*, 1804021.
(25) Bai, H.; Wu, Y.; Wang, Y.; Wu, Y.; Li, R.; Cheng, P.; Zhang, M.; Wang, J.; Ma, W.; Zhan, X. Nonfullerene acceptors based on extended fused rings flanked with benzothiadiazolylmethylenemalononitrile for polymer solar cells. *J. Mater. Chem. A* **2015**, *3*, 20758−20766.
(26) Wang, K.; Firdaus, Y.; Babics, M.; Cruciani, F.; Saleem, Q.; El Labban, A.; Alamoudi, M. A.; Marszalek, T.; Pisula, W.; Laquai, F.; Beaujuge, P. M. π-Bridge-Independent 2-(Benzo[c][1,2,5]thiadiazol-4-ylmethylene)malononitrile-Substituted Nonfullerene Acceptors for Efficient Bulk Heterojunction Solar Cells. *Chem. Mater.* **2016**, *28*, 2200−2208.
(27) Tan, C.-H.; Gorman, J.; Wadsworth, A.; Holliday, S.; Subramaniyan, S.; Jenekhe, S. A.; Baran, D.; McCulloch, I.; Durrant, J. R. Barbiturate end-capped non-fullerene acceptors for organic solar cells: tuning acceptor energetics to suppress geminate recombination losses. *Chem. Commun.* **2018**, *54*, 2966−2969.
(28) Lin, Y.; Wang, J.; Zhang, Z.-G.; Bai, H.; Li, Y.; Zhu, D.; Zhan, X. An Electron Acceptor Challenging Fullerenes for Efficient Polymer Solar Cells. *Adv. Mater.* **2015**, *27*, 1170−1174.
(29) Bai, H.; Wang, Y.; Cheng, P.; Wang, J.; Wu, Y.; Hou, J.; Zhan, X. An electron acceptor based on indacenodithiophene and 1,1-dicyanomethylene-3-indanone for fullerene-free organic solar cells. *J. Mater. Chem. A* **2015**, *3*, 1910−1914.
(30) Lee, J.; Ko, S.-J.; Lee, H.; Huang, J.; Zhu, Z.; Seifrid, M.; Vollbrecht, J.; Brus, V. V.; Karki, A.; Wang, H.; Cho, K.; Nguyen, T.-Q.; Bazan, G. C. Side-Chain Engineering of Nonfullerene Acceptors for Near-Infrared Organic Photodetectors and Photovoltaics. *ACS Energy Lett.* **2019**, *4*, 1401−1409.
(31) Firdaus, Y.; Le Corre, V. M.; Khan, J. I.; Kan, Z.; Laquai, F.; Beaujuge, P. M.; Anthopoulos, T. D. Key Parameters Requirements for Non-Fullerene-Based Organic Solar Cells with Power Conversion Efficiency > 20%. *Adv. Sci.* **2019**, *6*, 1802028.
(32) Zhou, N.; Facchetti, A. Naphthalenediimide (NDI) polymers for all-polymer photovoltaics. *Mater. Today* **2018**, *21*, 377−390.
(33) Sun, H.; Wang, L.; Wang, Y.; Guo, X. Imide-Functionalized Polymer Semiconductors. *Chem. - Eur. J.* **2019**, *25*, 87−105.
(34) Guo, X.; Kim, F. S.; Seger, M. J.; Jenekhe, S. A.; Watson, M. D. Naphthalene Diimide-Based Polymer Semiconductors: Synthesis, Structure-Property Correlations, and n-Channel and Ambipolar Field-Effect Transistors. *Chem. Mater.* **2012**, *24*, 1434−1442.
(35) Zhan, X.; Facchetti, A.; Barlow, S.; Marks, T. J.; Ratner, M. A.; Wasielewski, M. R.; Marder, S. R. Rylene and Related Diimides for Organic Electronics. *Adv. Mater.* **2011**, *23*, 268−284.
(36) Würthner, F. Perylene bisimide dyes as versatile building blocks for functional supramolecular architectures. *Chem. Commun.* **2004**, 1564−1579.
(37) Yan, Q.; Zhou, Y.; Zheng, Y.-Q.; Pei, J.; Zhao, D. Towards rational design of organic electron acceptors for photovoltaics: a study based on perylenediimide derivatives. *Chem. Sci.* **2013**, *4*, 4389−4394.
(38) Park, G. E.; Kim, H. J.; Choi, S.; Lee, D. H.; Uddin, M. A.; Woo, H. Y.; Cho, M. J.; Choi, D. H. New M- and V-shaped perylene diimide small molecules for high-performance nonfullerene polymer solar cells. *Chem. Commun.* **2016**, *52*, 8873−8876.
(39) Wang, J.; Zhan, X. Rylene Diimide Electron Acceptors for Organic Solar Cells. *Trends in Chemistry* **2019**, *1*, 869.
(40) He, Q.; Li, T.; Yan, C.; Liu, Y.; Wang, J.; Wang, M.; Lin, Y.; Zhan, X. Cracking perylene diimide backbone for fullerene-free polymer solar cells. *Dyes Pigm.* **2016**, *128*, 226−234.
(41) Liu, Y.; Zhang, L.; Lee, H.; Wang, H.-W.; Santala, A.; Liu, F.; Diao, Y.; Briseno, A. L.; Russell, T. P. NDI-Based Small Molecule as Promising Nonfullerene Acceptor for Solution-Processed Organic Photovoltaics. *Adv. Energy Mater.* **2015**, *5*, 1500195.
(42) Rundel, K.; Maniam, S.; Deshmukh, K.; Gann, E.; Prasad, S. K. K.; Hodgkiss, J. M.; Langford, S. J.; McNeill, C. R. Naphthalene diimide-based small molecule acceptors for organic solar cells. *J. Mater. Chem. A* **2017**, *5*, 12266−12277.
(43) Li, H.; Kim, F. S.; Ren, G.; Hollenbeck, E. C.; Subramaniyan, S.; Jenekhe, S. A. Tetraazabenzodifluoranthene Diimides: Building Blocks for Solution-Processable n-Type Organic Semiconductors. *Angew. Chem., Int. Ed.* **2013**, *52*, 5513−5517.
(44) Li, H.; Hwang, Y.-J.; Courtright, B. A. E.; Eberle, F. N.; Subramaniyan, S.; Jenekhe, S. A. Fine-Tuning the 3D Structure of Nonfullerene Electron Acceptors Toward High-Performance Polymer Solar Cells. *Adv. Mater.* **2015**, *27*, 3266−3272.
(45) Hamonnet, J.; Nakano, M.; Nakano, K.; Sugino, H.; Takimiya, K.; Tajima, K. Bis(naphthothiophene diimide)indacenodithiophenes as Acceptors for Organic Photovoltaics. *Chem. Mater.* **2017**, *29*, 9618−9622.
(46) Li, S.; Liu, W.; Li, C.-Z.; Lau, T.-K.; Lu, X.; Shi, M.; Chen, H. A non-fullerene acceptor with a fully fused backbone for efficient polymer solar cells with a high open-circuit voltage. *J. Mater. Chem. A* **2016**, *4*, 14983−14987.
(47) Lin, Y.; Wang, J.; Dai, S.; Li, Y.; Zhu, D.; Zhan, X. A Twisted Dimeric Perylene Diimide Electron Acceptor for Efficient Organic Solar Cells. *Adv. Energy Mater.* **2014**, *4*, 1400420.
(48) Zhang, Y.; Guo, X.; Guo, B.; Su, W.; Zhang, M.; Li, Y. Nonfullerene Polymer Solar Cells based on a Perylene Monoimide Acceptor with a High Open-Circuit Voltage of 1.3 V. *Adv. Funct. Mater.* **2017**, *27*, 1603892.
(49) Huang, C.; Liao, X.; Gao, K.; Zuo, L.; Lin, F.; Shi, X.; Li, C.-Z.; Liu, H.; Li, X.; Liu, F.; Chen, Y.; Chen, H.; Jen, A. K. Y. Highly Efficient Organic Solar Cells Based on S, N-Heteroacene Non-Fullerene Acceptors. *Chem. Mater.* **2018**, *30*, 5429−5434.
(50) Zhao, W.; Qian, D.; Zhang, S.; Li, S.; Inganäs, O.; Gao, F.; Hou, J. Fullerene-Free Polymer Solar Cells with over 11% Efficiency and Excellent Thermal Stability. *Adv. Mater.* **2016**, *28*, 4734−4739.
(51) Qiu, N.; Zhang, H.; Wan, X.; Li, C.; Ke, X.; Feng, H.; Kan, B.; Zhang, H.; Zhang, Q.; Lu, Y.; Chen, Y. A New Nonfullerene Electron Acceptor with a Ladder Type Backbone for High-Performance Organic Solar Cells. *Adv. Mater.* **2017**, *29*, 1604964.
(52) Li, H.; Earmme, T.; Subramaniyan, S.; Jenekhe, S. A. Bis(Naphthalene Imide)diphenylanthrazolines: A New Class of Electron Acceptors for Efficient Nonfullerene Organic Solar Cells and Applicable to Multiple Donor Polymers. *Adv. Energy Mater.* **2015**, *5*, 1402041.
(53) Xu, Y.-X.; Chueh, C.-C.; Yip, H.-L.; Ding, F.-Z.; Li, Y.-X.; Li, C.-Z.; Li, X.; Chen, W.-C.; Jen, A. K.-Y. Improved Charge Transport

DOI: 10.1021/acs.chemmater.9b03329
Chem. Mater. 2020, 32, 195−204

and Absorption Coefficient in Indacenodithieno[3,2-b]thiophene-based Ladder-Type Polymer Leading to Highly Efficient Polymer Solar Cells. *Adv. Mater.* **2012**, *24*, 6356−6361.
(54) Neculqueo, G.; Rojas Fuentes, V.; López, A.; Matute, R.; Vásquez, S. O.; Martínez, F. Electronic properties of thienylene vinylene oligomers: synthesis and theoretical study. *Struct. Chem.* **2012**, *23*, 1751−1760.
(55) Más-Montoya, M.; Janssen, R. A. J. The Effect of H- and J-Aggregation on the Photophysical and Photovoltaic Properties of Small Thiophene-Pyridine-DPP Molecules for Bulk-Heterojunction Solar Cells. *Adv. Funct. Mater.* **2017**, *27*, 1605779.
(56) Nilsson, K. P. R.; Rydberg, J.; Baltzer, L.; Inganäs, O. Self-assembly of synthetic peptides control conformation and optical properties of a zwitterionic polythiophene derivative. *Proc. Natl. Acad. Sci. U. S. A.* **2003**, *100*, 10170.
(57) Lee, S. K.; Zu, Y.; Herrmann, A.; Geerts, Y.; Müllen, K.; Bard, A. J. Electrochemistry, Spectroscopy and Electrogenerated Chemiluminescence of Perylene, Terrylene, and Quaterrylene Diimides in Aprotic Solution. *J. Am. Chem. Soc.* **1999**, *121*, 3513−3520.
(58) Zhu, Y.; Kulkarni, A. P.; Wu, P.-T.; Jenekhe, S. A. New Ambipolar Organic Semiconductors. 1. Synthesis, Single-Crystal Structures, Redox Properties, and Photophysics of Phenoxazine-Based Donor-Acceptor Molecules. *Chem. Mater.* **2008**, *20*, 4200−4211.
(59) Liu, T.; Troisi, A. What Makes Fullerene Acceptors Special as Electron Acceptors in Organic Solar Cells and How to Replace Them. *Adv. Mater.* **2013**, *25*, 1038−1041.
(60) Ren, G.; Schlenker, C. W.; Ahmed, E.; Subramaniyan, S.; Olthof, S.; Kahn, A.; Ginger, D. S.; Jenekhe, S. A. Photoinduced Hole Transfer Becomes Suppressed with Diminished Driving Force in Polymer-Fullerene Solar Cells While Electron Transfer Remains Active. *Adv. Funct. Mater.* **2013**, *23* (10), 1238−1249.
(61) Courtright, B. A.; Jenekhe, S. A. Polyethylenimine Interfacial Layers in Inverted Organic Photovoltaic Devices: Effects of Ethoxylation and Molecular Weight on Efficiency and Temporal Stability. *ACS Appl. Mater. Interfaces* **2015**, *7*, 26167−75.
(62) Proctor, C. M.; Kuik, M.; Nguyen, T.-Q. Charge carrier recombination in organic solar cells. *Prog. Polym. Sci.* **2013**, *38*, 1941−1960.
(63) Credgington, D.; Jamieson, F. C.; Walker, B.; Nguyen, T.-Q.; Durrant, J. R. Quantification of Geminate and Non-Geminate Recombination Losses within a Solution-Processed Small-Molecule Bulk Heterojunction Solar Cell. *Adv. Mater.* **2012**, *24*, 2135−2141.
(64) Stübinger, T.; Brütting, W. Exciton diffusion and optical interference in organic donor-acceptor photovoltaic cells. *J. Appl. Phys.* **2001**, *90*, 3632−3641.
(65) Babel, A.; Jenekhe, S. A. High Electron Mobility in Ladder Polymer Field-Effect Transistors. *J. Am. Chem. Soc.* **2003**, *125*, 13656−13657.
(66) Kim, F. S.; Park, C. H.; Na, Y.; Jenekhe, S. A. Effects of ladder structure on the electronic properties and field-effect transistor performance of Poly(benzobisimidazobenzophenanthroline). *Org. Electron.* **2019**, *69*, 301−307.
(67) Li, S.; Ye, L.; Zhao, W.; Zhang, S.; Mukherjee, S.; Ade, H.; Hou, J. Energy-Level Modulation of Small-Molecule Electron Acceptors to Achieve over 12% Efficiency in Polymer Solar Cells. *Adv. Mater.* **2016**, *28*, 9423−9429.
(68) Qian, D.; Ye, L.; Zhang, M.; Liang, Y.; Li, L.; Huang, Y.; Guo, X.; Zhang, S.; Tan, Z. a.; Hou, J. Design, Application, and Morphology Study of a New Photovoltaic Polymer with Strong Aggregation in Solution State. *Macromolecules* **2012**, *45*, 9611−9617.

DOI: 10.1021/acs.chemmater.9b03329
Chem. Mater. 2020, 32, 195−204